CONF-9609112--1

UCRL-JC-123762
PREPRINT

Synthetic Strong Ground Motions for Engineering Design Utilizing Empirical Green's Functions

L.J. Hutchings
S.P. Jarpe
P.W. Kasameyer
W. Foxall

This was prepared for submittal to the
Eleventh World Conference on Earthquake Engineering
Acapulco, Mexico
September 12, 1996

April 11, 1996

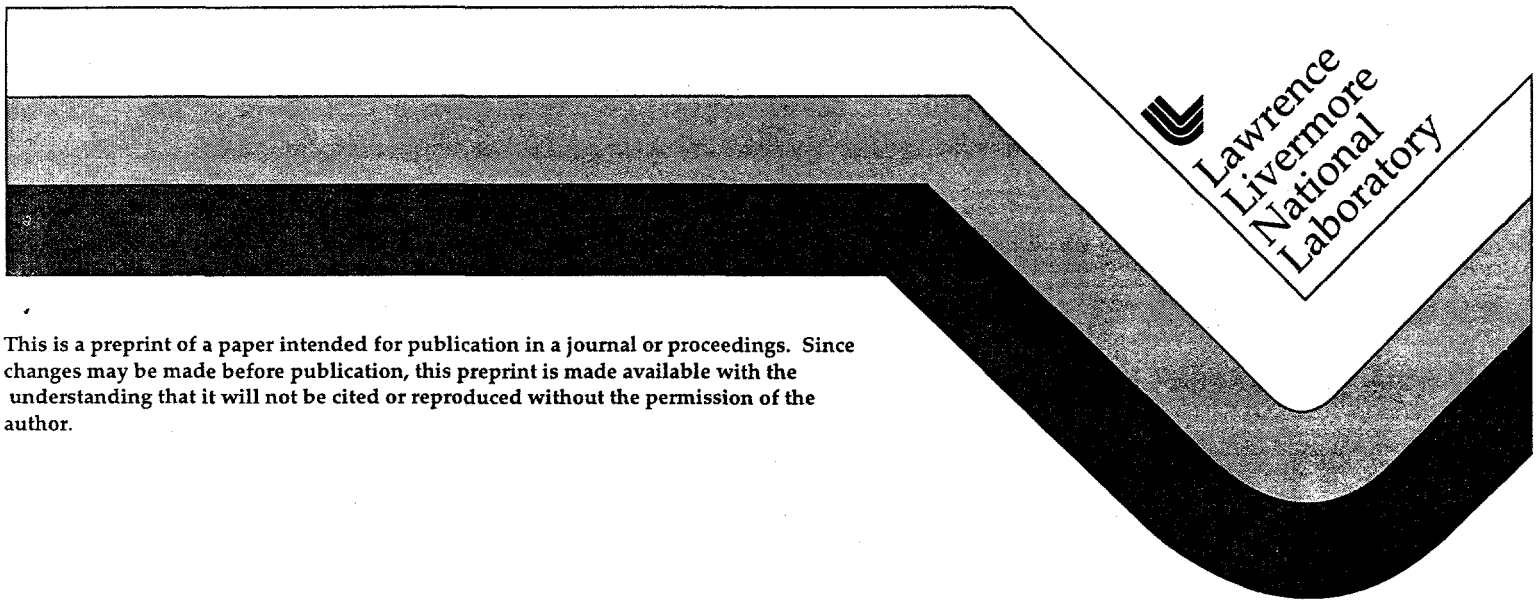

SYNTHETIC STRONG GROUND MOTIONS FOR ENGINEERING DESIGN UTILIZING EMPIRICAL GREEN'S FUNCTIONS

L.J. HUTCHINGS, S.P. JARPE, P.W. KASAMEYER, and W. FOXALL

Earth Sciences Department
Lawrence Livermore National Laboratory
Livermore, California 94551

ABSTRACT

We present a methodology for developing realistic synthetic strong ground motions for specific sites from specific earthquakes. We analyzed the possible ground motion resulting from a $M = 7.25$ earthquake that ruptures 82 km of the Hayward fault for a site 1.4 km from the fault in the eastern San Francisco Bay area. We developed a suite of 100 rupture scenarios for the Hayward fault earthquake and computed the corresponding strong ground motion time histories. We synthesized strong ground motion with physics-based solutions of earthquake rupture and applied physical bounds on rupture parameters. By having a suite of rupture scenarios of hazardous earthquakes for a fixed magnitude and identifying the hazard to the site from the statistical distribution of engineering parameters, we introduce a probabilistic component into the deterministic hazard calculation. Engineering parameters of synthesized ground motions agree with those recorded from the 1995 Kobe, Japan and the 1992 Landers, California earthquakes at similar distances and site geologies.

KEYWORDS

Synthetic ground motion; strong ground motion; empirical Green's functions; Hayward Fault; engineering parameters; hazard calculation

INTRODUCTION

We present a methodology for developing realistic synthetic strong ground motions for specific sites from specific earthquakes. Realistic time histories should be used for nonlinear dynamic analysis of structures (McCallen and Hutchings, 1996). We analyzed the possible ground motion from a $M = 7.25$ earthquake that ruptures 82 km of the Hayward fault for a site (BKS) 1.4 km from the fault in the eastern San Francisco Bay area. Figure 1 shows the location of the site and of the Hayward fault. We developed a suite of 100 rupture scenarios for the Hayward fault earthquake and computed the corresponding strong ground motion time histories. The scenarios were developed by randomly varying rupture parameters within a range of physical limits obtained from independent research. This approach is useful if (as is the case here) the range of possible fault rupture histories is narrow enough to functionally constrain the predicted strong ground motions. Log-normal average and one standard deviation (1σ) values of peak acceleration and absolute acceleration response spectra were derived from the suite of 100 synthesized strong ground motions. By having a suite of rupture scenarios of hazardous earthquakes for a fixed magnitude and identifying the

hazard to the site from a statistical analysis of engineering parameters, we have introduced a probabilistic component to the deterministic hazard calculation.

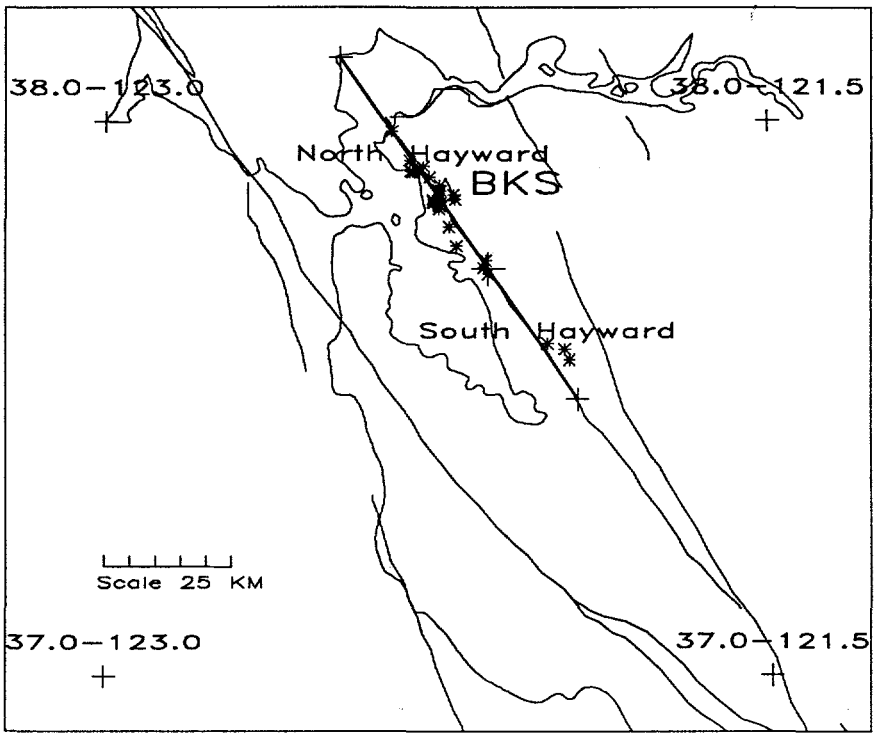

Fig. 1. Location of the site (BKS) and the two segments of the Hayward for the rupture model (crosses indicate ends of segments).

A realistic synthesis of ground motion should include the effects of geologic conditions along the propagation path from the fault to the site and at the site itself. These conditions can significantly amplify the seismic energy reaching a receiver and can focus and scatter energy. At sites close to large faults it is also critical to account for the effects of finite fault rupture. These effects include seismic arrivals radiated from portions of the fault that can be tens of kilometers apart and arrive at the same time, and directivity effects that can significantly increase or decrease wave field amplitudes. The superposition of direct and scattered body waves and surface waves will result in an extremely complicated wave field and should be modeled. To model all these effects, we synthesize strong ground motion with physics-based solutions of earthquake rupture that utilize empirical Green's functions and apply physics-based rupture parameters. Empirical Green's functions are defined here as recordings of effectively impulsive point source events (Hutchings and Wu, 1990). We have developed an exact solution to the representation relation for finite rupture that utilizes either empirical or synthetic Green's functions (Hutchings and Wu, 1990; Jarpe and Kasameyer, 1996). Here, we use recordings of small earthquakes to provide empirical Green's functions for frequencies $0.5 \leq f \leq 5$ Hz, and analytical calculations to provide synthetic Green's functions for $0.05 \leq f \leq 0.5$ Hz. We synthesize the entire wavetrain for three components (Hutchings, 1988). Although site soil can significantly affect ground motions with nonlinear effects, here we present only linear ground motions that might be expected at a rock outcrop.

We model the rupture process as a continuous rupture over fault segments with variable slip amplitude. This model is consistent, within the frequency range of resolution, with inversion studies (Kanamori, 1986; Wald *et al.*, 1990, 1993, 1995; Beroza and Spudich, 1988; Hartzel and Heaton, 1988; Hartzell 1989) and with what is known from dynamic rupture models about how earthquakes rupture (Rice, 1983; Kostrov and Das, 1988). Although these studies resolve fault slip histories only up to spatial resolutions of a few kilometers and only for $f \leq 1$ Hz, our method provides good fits to observed seismograms up to 25 Hz when these models are used (Jarpe and Kasameyer, 1996). The complexity added to rupture by many ground motion

synthesis approaches is not necessary to synthesize observed seismograms, and there is no evidence that earthquake rupture is highly complex at short spatial or temporal dimensions.
Most empirical Green's function synthesis approaches model fault rupture as highly complex by using a composite model whereby many small earthquakes (significantly larger than point sources) rupture independently over the fault surface (Irikura, 1983; Papageorgiou and Aki, 1983; Munguia and Brune, 1984; Joyner and Boore, 1986; Boatwright, 1988; Wennerberg, 1990; Aki and Irikura, 1991). There is little evidence for composite models of earthquakes. Also, composite models of faulting rely on scaling relations of earthquakes to determine the number of small earthquakes necessary to synthesize a large earthquake, and have difficulty matching the low and high frequency portions of synthesized seismograms to observed records (Joyner and Boore, 1986; Boatwright, 1988; Tumarkin *et al.*, 1994; Frankel, 1995). Our approach requires only that the number of small earthquakes used in the synthesis is such that the sum of their moments equal the moment of the large earthquake, which matches the low-frequency portion of observed seismograms. The high-frequency portion is matched by using appropriate rupture parameters (Hutchings, 1994).

GREEN'S FUNCTIONS

Empirical Green's functions have a better accuracy at high frequencies, where geologic inhomogeneities are not well modeled, and the synthetic Green's functions have better accuracy at lower frequencies, where empirical Green's functions do not have sufficient energy. The methods overlap in the frequency range $0.5 \leq f \leq 1$ Hz, where the geology can be modeled with some accuracy and the empirical Green's function have enough energy to be well recorded.

We computed synthetic Green's functions using the reflectivity method of Kennett (1983). This solution extends to $f = 0$ but does not include near-field terms. The focal mechanism radiation pattern is used for synthetic Green's functions solutions to the finite rupture. We considered only solutions for $f > 0.05$ Hz (period = 20 s), because lack of near-field arrivals diminishes the reliability of solutions for lower frequencies. Consistent with the work of Fuis and Mooney (1990), we used a 1-D velocity model with layer thicknesses of 4, 7, 11, and 23 km and with P-wave velocities of 4.5, 5.5, 6.0, 6.5, and (for the mantle) 8.0 km/s, respectively.

Empirical Green's functions should be recorded at the site of interest and from source events along the faults of interest, since site response and near-source propagation-path effects are highly variable. Empirical Green's functions include the actual effects of velocity structure, attenuation, and geometrical spreading. In this study the empirical Green's functions used are recordings of small earthquakes from the Berkeley broadband site (BKS: 37.877N, 122.235W).

It is not possible to record empirical Green's functions from all locations along a fault of interest and with the same focal mechanism solution, so source locations of empirical Green's functions were interpolated to fill in the fault. Figure 1 shows epicenter locations of source events used for empirical Green's functions. The spatial dependence of empirical Green's functions has been studied by Hutchings and Wu (1990), who found that the variability in ground motion arising from differences in source location and/or focal mechanism solutions is much less than that due to site response. Hutchings (1991, 1994) and Jarpe and Kasameyer (1996) found that interpolation for different source locations along a fault works quite well. Source events can be located near the fault of interest and need not lie directly along the fault. In synthesis, we have the option of correcting for different focal mechanism solutions, but Hutchings and Wu (1990) and Jarpe and Kasameyer (1996) found that for high frequencies such correction does not improve the synthesis. Interpolation is performed by correcting for attenuation, 1/R, and P- and S-wave arrival times due to differences in source distance. We include the radiation pattern effect for low frequencies when we use synthetic Green's functions. The velocity model used for interpolation and for focal mechanism corrections is $V_p = 4.0 + 0.182H$. The velocity closely approximates the model discussed above in the depth range 0 to 13 km, where the primary rupture and source events for empirical Green's functions occur.

HAYWARD FAULT RUPTURE

The Working Group on California Earthquake Probabilities (1988, 1990) identified northern and southern segments of the Hayward fault (Fig. 1), which are 50 and 32 km long, respectively, that are each capable of a magnitude 7.0 earthquake. We consider here the hazard from both segments rupturing during the same earthquake. We model the combined rupture as a $M = 7.25$ earthquake (moment magnitude; Hanks and Kanamori, 1979) that is linear sum of the two segments (Schwartz and Coppersmith, 1984; Sieh, 1984). The northern segment extends through northern San Francisco Bay; this is supported by recent high-resolution seismic profiles and seismicity (Lienkaemper *et al.*, 1991). South of the south segment, the fault has weak or nonexistent surface expression and very little microearthquake activity, and significant rupture is not expected (Working Group, 1990).

Two earthquakes occurred along the Hayward fault in the past century (1836 and 1868); the Working Group estimated both to have magnitude about 7.0. Slip rate estimates of about 9 mm/yr result in 1.4 m of accumulated strain since 1836 for the northern segment. Release of this strain is possible in the near future (Wells and Coppersmith, 1994).

RUPTURE MODELS

Our earthquake rupture models rely on moment, fault geometry, hypocenter, rupture roughness, rupture velocity, healing velocity, slip vector, and asperity location. Moment and fault geometry (extent of rupture and its orientation) are held fixed, while the other parameters were allowed to vary within limits. The fault rupture surface area was discretized into 0.01-km^2 elemental areas, which are small enough that modeled rupture is continuous for $f \leq 5$ Hz. The rupture initiates at the hypocenter and propagates radially at some fraction of the shear wave velocity. We used the Kostrov slip function to calculate the slip at a point; we approximated the shape as a ramp. We arbitrarily limited the rupture propagation factor in the Kostrov slip function to be equal to or less than the rupture time to the closest fault edge from the hypocenter. To develop 100 scenarios, we used a computer program that randomly varies independent rupture parameters subject to the following constraints. Other parameters are either held fixed or calculated from the rupture model.

ASPERITIES are included to add high slip amplitudes to portions of the rupture. Asperities are circular; their diameter is randomly chosen to be 0.2–0.8 times the fault width. The number of asperities is randomly selected for each scenario. Stress drops in asperity portions of rupture are higher than elsewhere.

ROUGHNESS is simulated as elements resisting rupture, then breaking. A percentage of elements (0, 10, 20, 33, or 50%) have rise times 10–90% those of neighboring elements, but with rupture completed at the same time as neighboring elements. These "rough" elements have correspondingly high stress drop.

MOMENT is constrained to be 8.0×10^{26} dyne-cm for the total rupture, including asperities. However, the moment of asperities is randomly selected, subject to the constraint that the maximum displacement is 5–10 m. Rigidity (proportional to shear wave velocity, except near the surface) diminishes near the surface so that the moment contribution diminishes. However, stress drop is also modeled to diminish (discussed below), so significant displacement can occur near the surface, although not seismogenic.

HYPOCENTER is constrained to occur at least 1 km from the fault ends, 2 km from the lower limit of the fault, and more than 7.5 km deep. The limit at the lower portion of the fault arises because the rigidity of material more than 13 km deep is modeled as decreasing as the aseismic zone is approached, and the limit to depths of more than 7.5 km is due to the observation that past earthquakes originate at depth.

RUPTURE VELOCITY is randomly selected to be from 0.75 to 1.0 times the shear wave velocity.

HEALING VELOCITY is the velocity for the stress pulse that terminates slip. The healing phase is initiated after the rupture front arrives at any fault edge. The free surface is not allowed to be a healing boundary for rupture, because significant seismic pulses that are necessary to shut down slip are not generated from the surface (Das and Kostrov, 1985; Scholz, 1990). The healing velocity is randomly selected to between 0.8 and 1.0 times the rupture velocity, which is between the Rayleigh and shear wave velocities.

RISE TIME is equal to the time it takes, after the initiation of rupture, for the first healing phase to arrive.

STRESS DROP is a dependent variable derived from the Kostrov slip function and allowed to vary due to three effects modeled in rupture. Asperities and rough rupture are allowed to have a different stress drop than surrounding portions of the fault rupture (discussed above). Also, stress drop is constrained to diminish near the surface of the earth at the rate of 10 + 0.75 times the confining pressure due to the lithostatic load (300 bars at 1.7 km depth). The minimum of the stress drop calculated using this constraint and the full rupture stress drop is used.

SLIP VECTOR is constrained to 180° for a right-lateral strike slip fault.

PREDICTION UNCERTAINTY

In the terminology of Abrahamson *et al.*, (1990), our prediction uncertainty has two elements: (1) parametric uncertainty, which arises from uncertainty as to which scenario will occur, and (2) modeling and random errors caused by not modeling the rupture process correctly and by factors such as uncertainties in moment estimates for empirical Green's functions and errors caused by interpolation of events along the fault surface.

We estimated the parametric uncertainty by generating a suite of time histories from 100 sets of the independent parameters. We selected these sets at random by assuming that the parameters are uncorrelated and that each is uniformly distributed through its allowed range. Figure 2 shows the average (in log space) of the absolute acceleration response (AAR) spectra for the two horizontal components calculated for each of the 100 parameter sets. All these parameter sets represent earthquakes with the same moment and fault rupture area, parameters that might be successfully anticipated in advance. It is clear from this figure that a broad range of possible response spectra could be generated from an event whose moment and fault rupture area are fixed.

We examine the AAR data at a single frequency (1 Hz) to illustrate how the parametric error can be estimated and how that estimate is improved by calculating more scenarios. Figure 3 is a histogram of the natural logarithms of the calculated values at that frequency. The data are distributed close to normally in log-space with a sample mean and standard deviation of –0.44 and 0.80, although they fail a χ^2 test (Freund, 1962) for the log normal distribution. Figure 4 shows the evolution of sample mean as a function of the number of scenarios run. The uncertainty in the mean is estimated from the observed variability and the number of points used, approximating the data-distribution as log-normal. A similar calculation was made for the "84th percentile" represented by the sum of the sample mean and sample standard deviation. The uncertainty in the sum is estimated by assuming the errors in the mean and standard deviation are independent (Hald, 1952). Estimates of the mean and 84th percentile vary significantly with the number of scenarios, but the final estimates (for 100 scenarios) always lie within the 1σ bounds for the estimate uncertainty, suggesting that the approximate error model gives a useful estimate of the uncertainty. The uncertainties decrease significantly as more scenarios are added. The uncertainty in the natural logarithm of the mean decreased from 0.29 after 10 scenarios, to 0.08 (corresponding to approximately $\pm 0.05g$) after 100. The bounds for the 84th percentile are about $\pm 0.18g$ after 100 runs. Given enough computer time, we can determine the parametric uncertainty to any accuracy desired. For example, the uncertainties in the mean and 84th percentiles would be reduced to $\pm 0.016g$ and $\pm 0.06g$, respectively, if we ran 1000 scenarios.

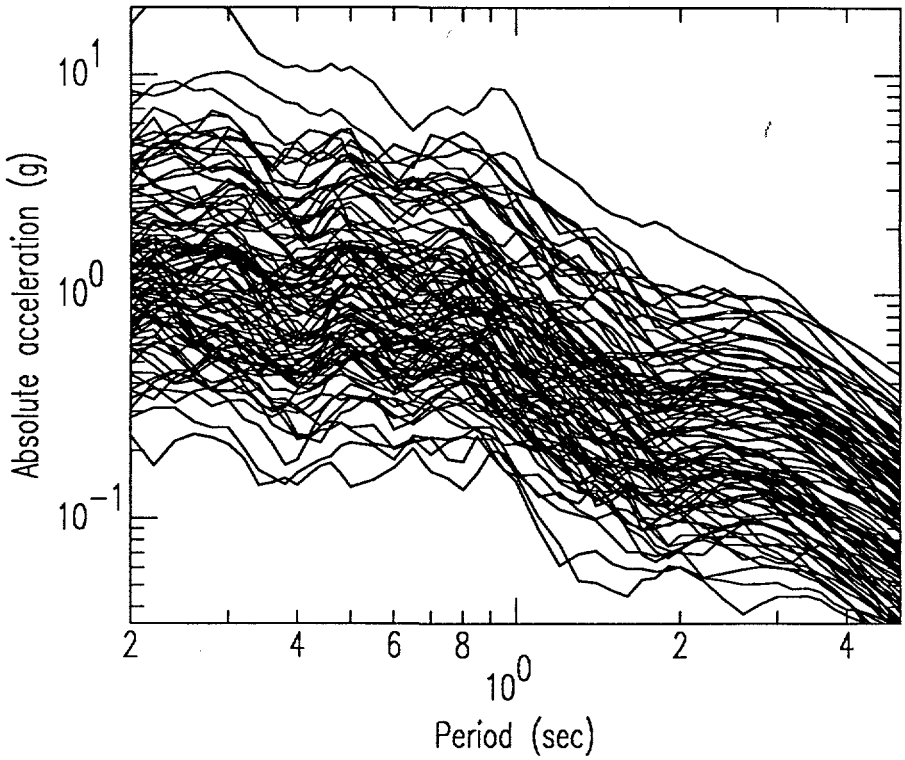

Fig. 2. Absolute acceleration response at 5% damping for the 100 scenarios.

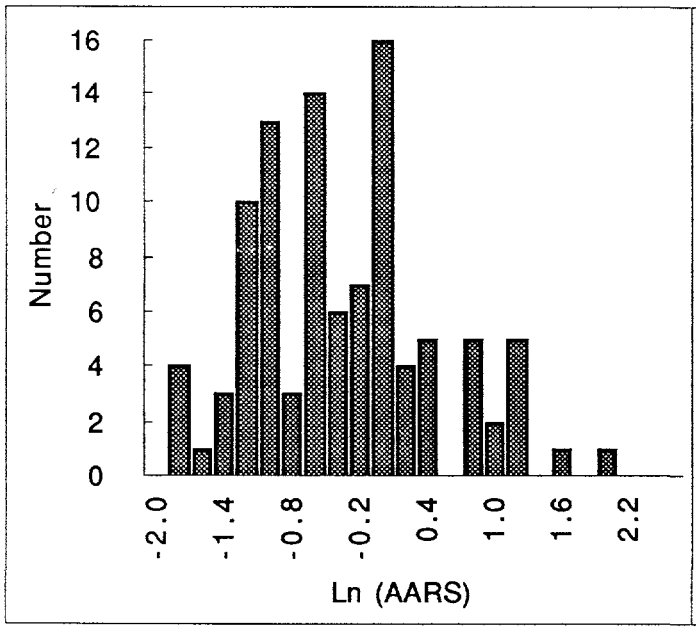

Fig. 3. Histogram of number of scenarios as a function of AAR at 1.0 s.

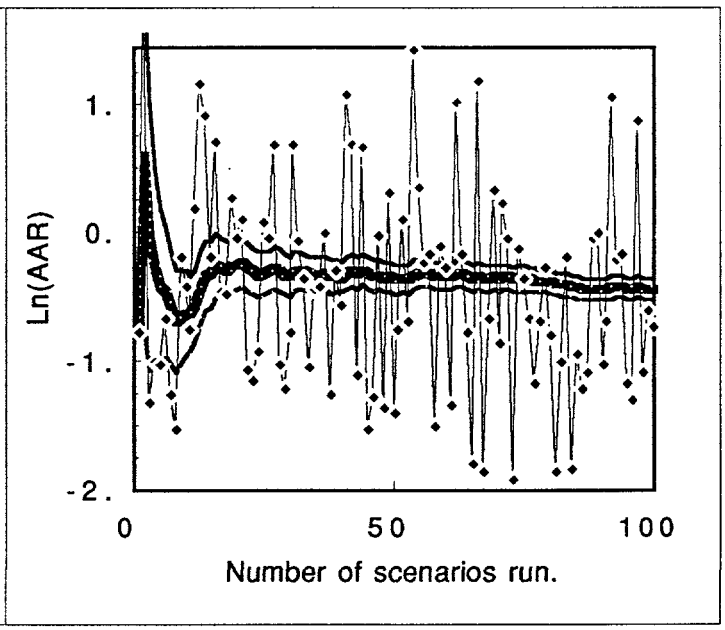

Fig. 4. Estimation of the mean (dark line) AAR at 1.0 s, its uncertainty, and individual AAR values, vs number of scenarios run.

Jarpe and Kasameyer (1996) estimated the second element of uncertainty, modeling and random error, by comparing computed and observed records for the 1989 Loma Prieta earthquake, whose independent parameters were well determined. The total source uncertainty is characterized by adding the parametric and "random plus modeling" standard deviation estimates (0.80 and 0.55 at 1 Hz) in quadrature. The mean and 84th percentiles of the AAR distribution calculated in this manner are given by the dark lines in Figure 5.

HAZARD

A methodology for identifying the ground motion hazard to a site is to choose an acceptable probability from the suite of hazards from the 100 rupture scenarios. If either the mean or $+1\sigma$ AAR (50th or 84th pertentile) is chosen to identify the hazard, then time histories with AAR near these values would represent the hazard. It is not recommened to modify AAR to match a "target" spectrum, because this would in effect alter the rupture scenario and may inadvertently generate a non-physical model. Further, in non-linear structural analysis more than one time history should be selected. Rupture models HAY83 and HAY16 generated time histories that had AAR closest to the mean and $+1\sigma$ values, respectively. Figure 5 shows these AAR along with those from two additional models that closely matched (HAY40 and HAY06 for mean values, and HAY42 and HAY69 for $+1\sigma$ values). Figure 6 shows the slip distribution and hypocenter for scenarios HAY83 and HAY16. Figure 7 shows their time histories; the top three are the three components of acceleration, the middle three are the same records integrated to velocity, and the bottom three are the displacements.

DISCUSSION AND CONCLUSIONS

Since BKS is adjacent to the fault, one expects a large fault normal component in long periods. This is evident in the velocity and displacement records in Fig. 7, where the top trace is aligned fault parallel and the second trace is fault normal. Table 1 lists fault normal and fault parallel values of peak acceleration and velocity from records of the 1992, M=7.3 Landers earthquakes at comperable distance and geology as BKS. Also listed is a computation for a site at 4.3 km from the Hayward fault (STK, Figure 6), which is at a comperable distance and geology as a recording from the 1995, M=6.9 Kobe, Japan earthquake (soils modeling provided by J.C. Chen, personal communication, 1996). It is apparent that the results at these two sites are close to those obtained for actual recordings and that the methodology provides a realistic predictive tool for a possible future Hawyard fault earthquake.

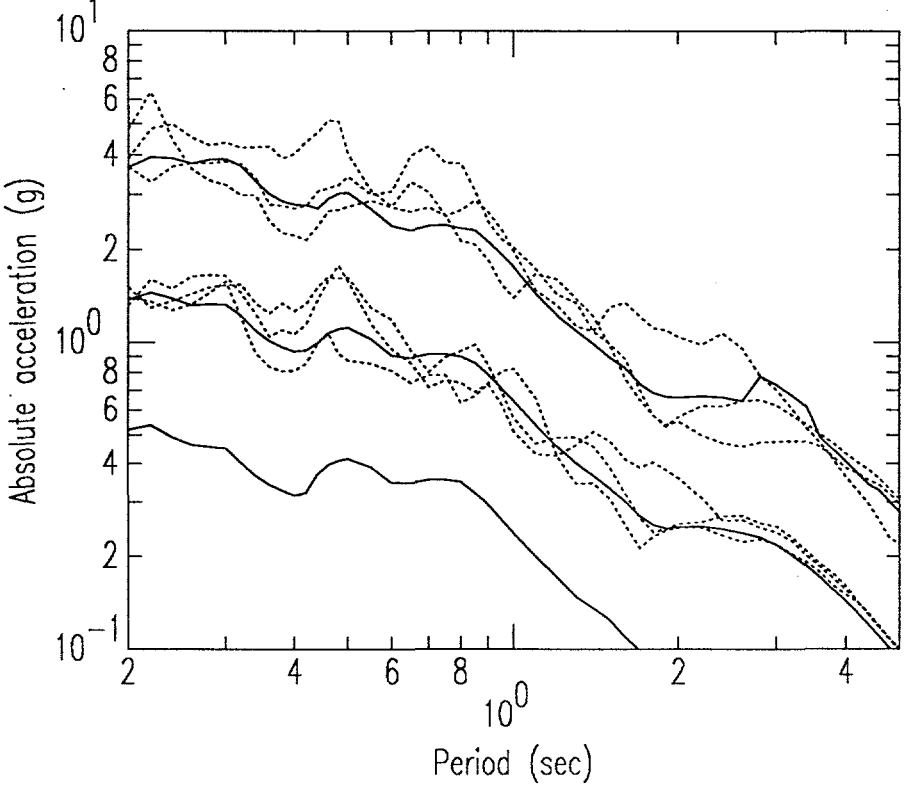

Fig. 5. The mean and $\pm$ 1 σ AAR estimated from the 100 rupture scenarios (solid lines,) and AAR from scenario earthquakes that have similar AAR (dotted line).

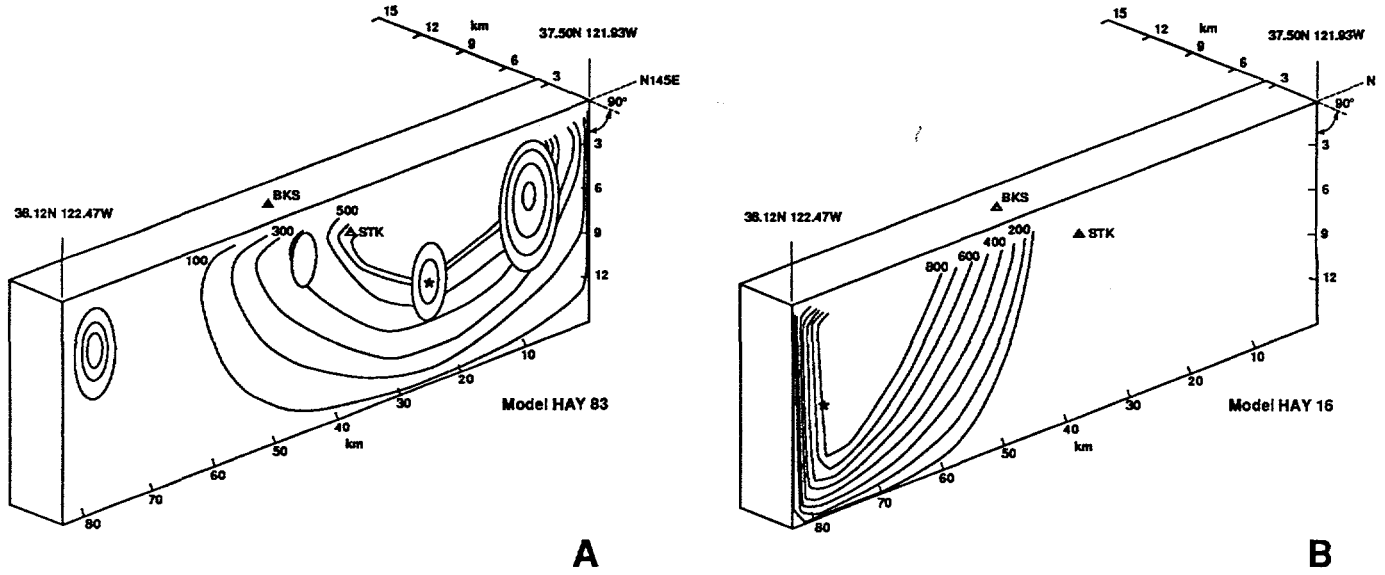

Fig. 6. (a). In-plane view of the fault for a scenario rupture that generated a AAR near the mean AAR. Contours are slip amplitude in centimeters. Hypocenter is indicated by an asterisk; two site locations are shown as triangles. (b) A scenario rupture that generated an AAR near the $+\sigma$ AAR.

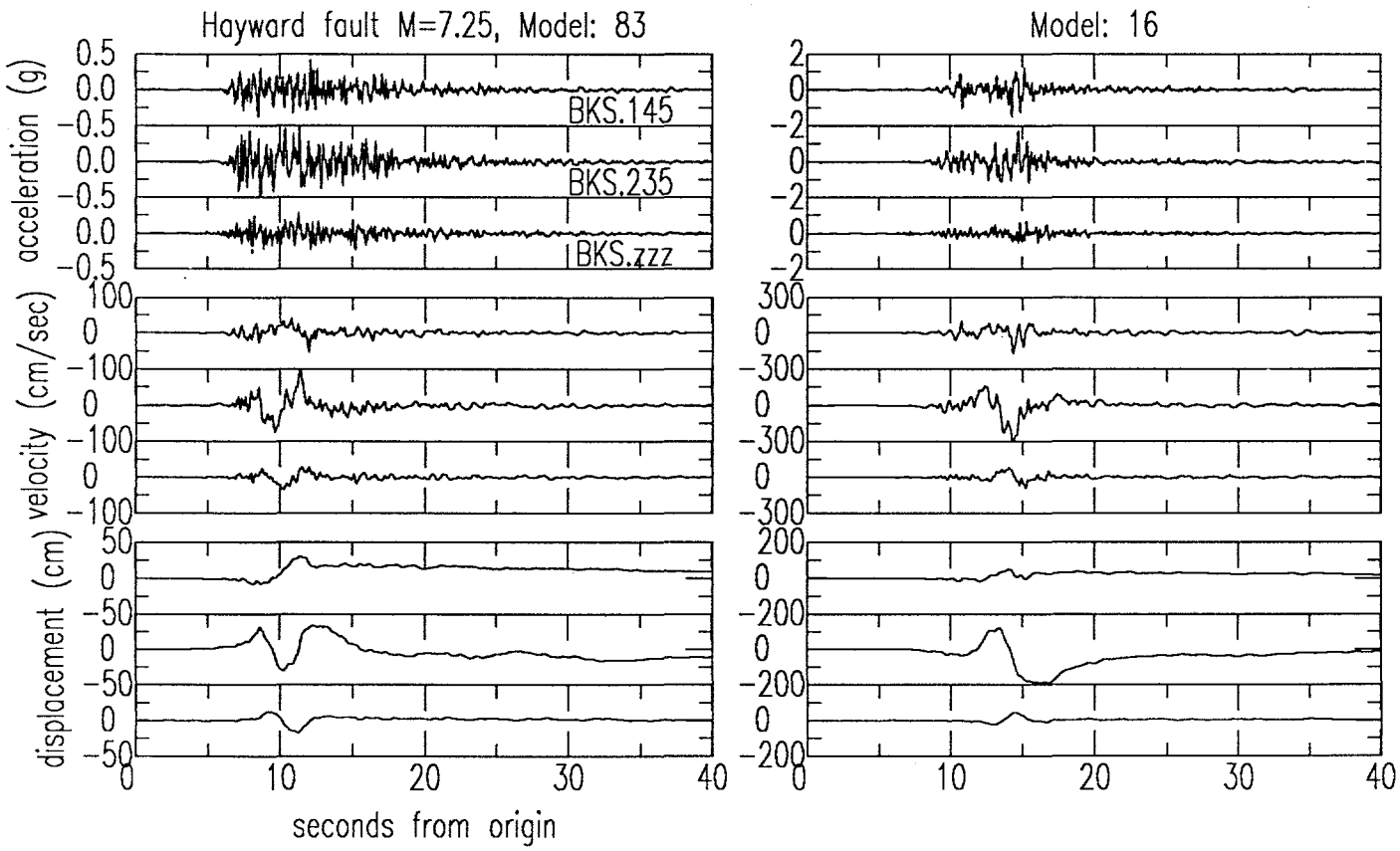

Fig. 7. Time histories for the a $+1\sigma$ AAR scenario. Top three are acceleration and the horizontal components are oriented as fault parallel (N145E) and fault normal (N235E). The middle three are velocity; note the large fault-normal pulse. The bottom three are displacements.

TABLE 1

Earthquake	Site geology	Distance	FN - FP peak accel		FN - FP peak vel	
Landers, 1992*	Lucerne,rock	1.1	0.76	0.73	127.5	95.3
Synthetic, mean HAY83	BKS, rock	1.4	0.5	0.4	100.0	45.0
Kobe, 1995*	Takatori,soil	4.3	0.81	0.42	174.9	62.7
Synthetic, $+1\sigma$ HAY	STK, soil	4.3	0.87	0.69	140.0	100.0

* data values from Somerville et al., (1995)

REFERENCES

Abrahamson, N.A., P.G. Somerville, and C.A. Cornell (1990). *Uncertainty in Numerical Strong Motion Predictions*. In: *Proc. 4th U.S. National Conf. Earthquake Engineering*, Vol. 1 (Earthquake Engineering Research Institute, 20–24 May, Palm Springs, California).

Aki, K. and K. Irikura (1991). Characterization and mapping of earthquake shaking for seismic zonation. In: *Proceedings of the Fourth International Conference on Seismic Zonation,* Vol. I, Earthquake Engineering Research Institute, Oakland, 61–110.

Beroza, G.C. and P. Spudich (1988). Linearized inversion for fault rupture behavior: application to the 1984 Morgan Hill, California earthquake. *J. Geophys. Res.* **93**, 6275–6296.

Boatwright, J. (1988). The seismic radiation from composite models of faulting, Bull. Seismol. Soc. Am. 78, 489–508.

Das, S. and B.V. Kostrov (1985). An elliptical asperity in shear: fracture process and seismic radiation. *Geophys. J. R. Astron. Soc.* **80**, 725–742.

Frankel, A. (1995). Simulating strong motion of large earthquakes using recordings of small earthquakes: the Loma Prieta main shock as a test case. *Bull. Seismol. Soc. Am.* **85**, 1144–1160.

Fuis, G.S. and W.D. Mooney (1990). Lithospheric structure and tectonics from seismic refraction and other data. In: *The San Andreas Fault System, California* (R.E. Wallace, ed.), U. S. Geological Survey Prof. Paper 1515, 207.

Freund, John E., Mathematical Statistics, 390 pp., Prentice-Hall, Englewood Cliffs, N.J., 1962

Hald, A., Statistical Theory with Engineering Applications, John Wiley and Sons, New York, 1952 (1952)

Hanks, T.C. and H. Kanamori (1979). A moment magnitude scale. *J. Geophys. Res.* **84**, 2348–2350.

Hartzell, S.H. (1989). Comparison of seismic waveform inversion results for the rupture history of a finite fault: application to the 1986 North Palm Springs, California earthquake. *J. Geophys. Res.* **94**, 7515–7534.

Hartzell, S.H. and T.H. Heaton (1988). Inversion of strong ground motion and teleseismic waveform data for the fault rupture history of the 1979 Imperial Valley, California, earthquake. *Bull. Seismol. Soc. Am.* **73**, 1533–1583.

Hutchings, L. (1988). Modeling strong earthquake ground motion with an earthquake simulation program EMPSYN that utilizes empirical Green's functions, Lawrence Livermore National Laboratory, Livermore, CA, UCRL-ID-105890, p. 122.

Hutchings, L. (1991). "Prediction" of strong ground motion for the 1989 Loma Prieta earthquake using empirical Green's functions. *Bull. Seismol. Soc. Am.* **81**, 88–121.

Hutchings, L. (1994). Kinematic earthquake models and synthesized ground motion using empirical green's functions. *Bull. Seismol. Soc. Am.* **84**, 1028–1050.

Hutchings, L. and F. Wu (1990). Empirical Green's functions from small earthquakes—A waveform study of locally recorded aftershocks of the San Fernando earthquake. *J. Geophys. Res.* **95**, 1187–1214.

Irikura, K. (1983). Semi-empirical estimation of strong ground motions during large earthquakes. *Bull. Disaster Prev. Res. Inst Kyoto Univ.* **33**, 63–104.

Jarpe, S.P. and P.W. Kasameyer (1996). Validation of a methodology for predicting broadband strong motion time histories from empirical green's functions. *Bull. Seismol. Soc. Am.,* in press.

Joyner, W.B. and D.M. Boore (1986). On simulating large earthquakes by Green's-function addition of smaller earthquakes. *Earthquake Source Mechanics,* Geophysical Monograph No. 37 (Maurice Ewing, ed.), **8**, 269–274.

Kanamori, H. (1986) Rupture process of subduction-zone earthquakes. *Ann .Rev .Earth .Planet .Sci.* **14**, 293-322.

Kennett, B.L.N. (1983). *Seismic Wave Propagation in Stratified Media,* Cambridge University Press, Cambridge.

Kostrov, B.V. and S. Das (1988). Principles of earthquake source mechanics. In: *Cambridge Monographs on Mechanics and Applied Mathematics*, Cambridge University Press, Cambridge.

Lienkaemper, J.J., G. Borchert, J.F. Wilmesher, and D. Meier (1989). Holocene slip rate along the Hayward fault, northern California. *EOS, Trans. Am. Geophys. Union* **70** (43), 1349.

McCallen, D.B. and L.J. Hutchings (1996). Ground motion estimation and nonlinear seismic analysis. Lawrence Livermore National Laboratory, Livermore, CA, UCRL-JC-121667. In press, proceedings: 12th Conference on Analysis and Computation of the American Society of Civil Engineers, Chicago,.

Munguia, L. and N.B. Brune (1984). Simulation of strong ground motion for earthquakes in the Mexicali–Imperial Valley region. *Geophys. J. R. Astron. Soc.* **79**, 747–771.

Papageorgiou, A.S. and K. Aki (1983). A specific barrier model for the quantitative description of inhomogeneous faulting and the prediction of strong ground motion. I. Description of the model. *Bull. Seismol. Soc. Am.* **73**, 693–722.

Rice, J.R. and A.L. Ruina (1983). Stability of steady friction slipping. *J. Appl. Mech.* **105**, 343–349.

Scholz, C.H. (1990). *The Mechanics of Earthquake Faulting*, Cambridge University Press, Cambridge.

Schwartz, D.P. and K.J. Coppersmith (1984). Fault behavior and characteristic earthquakes: Examples from the Wasatch and San Andreas faults. *J. Geophys. Res.* **89**, 5681–5698.

Sieh, K. (1984) Lateral offsets and revised dates of large prehistoric earthquakes at Pallet Creek, southern California. *J. Geophys. Res.* 89, 7641-7670.

Somerville, P. G., N. F. Smith, R. W. Graves, and N. A. Abrahamson (1995) Representation of near-fault rupture directivity effects in design ground motions, and applications to Caltrans bridges. in proceedings of the National Seismic Conference on Bridges and Highways.

Tumarkin, A.G., R.J. Archuleta, and R. Madariaga (1994). Basic scaling relations for composite models. *Bull. Seism. Soc. Am.* **84**, (4).

Wald, D.J., T.H. Heaton, and K.W. Hudnut (1995). The slip history of the 1994 Northridge, California earthquake determined from strong-motion, teleseismic, GPS, and leveling data (preprint). *Bull. Seismol. Soc. Am.* **81** (1).

Wald, D.J., D.V. Helmberger, and S.H. Hartzell (1990). Rupture process of the 1987 Superstition Hills Earthquake from inversion of strong-motion data. *Bull. Seismol. Soc. Am.* **80**, 1079–1098.

Wald, D.J., D.V. Helmberger, and T.H. Heaton (1991). Rupture model of the 1989 Loma Prieta earthquake from inversion of strong-motion and broadband teleseismic data. *Bull. Seismol. Soc. Am.* **81**, 1540–1572.

Wald, D.J., H. Kanamori, D.V. Helmberger, and T.H. Heaton (1993). Source study of the 1906 San Francisco earthquake. *Bull. Seismol. Soc. Am.* **83**, 981–1019.

Wennerberg, L. (1990). Stochastic summation of empirical Green's functions. *Bull. Seismol. Soc. Am.* **80**, 1418–1432.

Working Group on California Earthquake Probabilities (1990). *Probabilities of Large Earthquakes in the San Francisco Bay Region, California.* U.S. Geological Survey Circular 1053.

Working Group on California Earthquake Probabilities (1988). *Probabilities of Large Earthquakes in tCalifornia on the San Andreas fault.* . U.S. Geological Survey Open-file Report 88-398.

*This work was performed under the auspices of the U.S. Department of Energy by Lawrence Livermore National Laboratory under contract No. W-7405-Eng-48.